Biomechanical Properties of Abdominal Organs In Vivo and Postmortem Under Compression Loads

Jacob Rosen[1]
Department of Electrical Engineering,
University of Washington,
Box 352500,
Seattle, WA 98195-2500
e-mail: rosen@u.washington.edu

Jeffrey D. Brown[2]
e-mail: jdbrown@alumni.washington.edu

Smita De
e-mail: sd6@alumni.washington.edu

Department of Bioengineering,
University of Washington,
Box 352500,
Seattle, WA 98195-2500

Mika Sinanan
Department of Surgery,
University of Washington,
Box 356410,
Seattle, WA 98195-2500
e-mail: mssurg@u.washington.edu

Blake Hannaford
Department of Electrical Engineering,
University of Washington,
Box 352500,
Seattle, WA 98195-2500
e-mail: blake@u.washington.edu

Accurate knowledge of biomechanical characteristics of tissues is essential for developing realistic computer-based surgical simulators incorporating haptic feedback, as well as for the design of surgical robots and tools. As simulation technologies continue to be capable of modeling more complex behavior, an in vivo tissue property database is needed. Most past and current biomechanical research is focused on soft and hard anatomical structures that are subject to physiological loading, testing the organs in situ. Internal organs are different in that respect since they are not subject to extensive loads as part of their regular physiological function. However, during surgery, a different set of loading conditions are imposed on these organs as a result of the interaction with the surgical tools. Following previous research studying the kinematics and dynamics of tool/tissue interaction in real surgical procedures, the focus of the current study was to obtain the structural biomechanical properties (engineering stress-strain and stress relaxation) of seven abdominal organs, including bladder, gallbladder, large and small intestines, liver, spleen, and stomach, using a porcine animal model. The organs were tested in vivo, in situ, and ex corpus (the latter two conditions being postmortem) under cyclical and step strain compressions using a motorized endoscopic grasper and a universal-testing machine. The tissues were tested with the same loading conditions commonly applied by surgeons during minimally invasive surgical procedures. Phenomenological models were developed for the various organs, testing conditions, and experimental devices. A property database—unique to the literature—has been created that contains the average elastic and relaxation model parameters measured for these tissues in vivo and postmortem. The results quantitatively indicate the significant differences between tissue properties measured in vivo and postmortem. A quantitative understanding of how the unconditioned tissue properties and model parameters are influenced by time postmortem and loading condition has been obtained. The results provide the material property foundations for developing science-based haptic surgical simulators, as well as surgical tools for manual and robotic systems. [DOI: 10.1115/1.2898712]

Keywords: soft tissue, biomechanics, internal organs, surgical robotics, surgical simulation, haptics, surgical tools

1 Introduction

New technologies such as surgical robotics [1] and surgical simulators have fundamentally changed the practice of surgery in general and minimally invasive (laparoscopic) techniques, in particular. To date, there have been little biomechanical data available of soft tissue in vivo, and current simulators and robots have largely been designed to accomplish acceptable handling characteristics, as determined by subjective criteria.

Accurate models of clinically relevant tissues will allow prediction of manipulation forces and torques as well as potential damage to tissue as it is exposed to stresses applied by surgical tools.

Surgical training has been affected by many factors such as statutory limitation of work hours, patient safety concerns, and growing regulatory needs for credentialing of surgical trainees. Formal curriculum development with specific milestones and significant improvement in computer-based surgical simulation as a training tool have also augmented the surgical armamentarium. However, initial simulation efforts did not focus on the accuracy with which they render deformation, forces, and displacements of the tissues, and few provided any haptic feedback. As the next generation of simulators is developed, biomechanical data are essential for making this feedback accurate. The consequences of inaccurate tissue deformation modeling on clinical performance after simulation training have not been formally studied, but it is reasonable to assume that students accustomed to inaccurate forces or displacements from simulation training might put the patient at greater risk of tissue injury when applying their skills in the actual operating room. With few exceptions, most of the existing literature on the biomechanics of internal organ tissue comes from measurements taken from nonliving tissue. Physiologic changes in living tissue influence the mechanical properties of soft tissues. For example, the response of tissue to cyclic loading, due in part to the effect of fluid within the tissue, is stabilized after several similar loading cycles—a phenomenon known as conditioning [2]. Most experimental protocols used in other studies include tissue preconditioning in which tissue samples are exposed to 10–20 loading cycles before the measurements are recorded. This process runs counter to the normal conditions found

[1]Corresponding author.
[2]Present address: Intuitive Surgical, 1266 Kifer Road, Sunnyvale, CA 94086, USA.

Contributed by the Bioengineering Division of ASME for publication in the JOURNAL OF BIOMECHANICAL ENGINEERING. Manuscript received July 15, 2005; final manuscript received September 28, 2007; published online April 8, 2008. Review conducted by Andrew D McCulloch.

in surgery since surgeons do not typically "precondition" tissues before manipulating them. As a result, the tissues' biomechanical response to the first loading cycle has not been widely reported. The following paragraphs present a brief survey of the soft tissue testing literature.

Following the classic work on rabbit mesentery in uniaxial tension [3], in vitro tests of esophagus, stomach, small and large intestines, liver, and gallbladder under tension loads and failure levels of both animal and human cadaveric tissues were reported [4–6]. Several studies describe testing abdominal organs in relation to blunt impact injury, especially in the context of automobile accidents (for review, see Refs. [7,8,18,46]). More detailed measurements of specific organs included shear measurements of liver [9–11], and distension of intestine (relation between pressure and volume) [12,13]. In the context of laparoscopic surgery, the uniaxial force as well as displacements required to puncture pig and sheep liver and spleen with a scalpel were reported [14–16]. Elastic and stress-relaxation properties of porcine liver, spleen, and kidney were studied in vitro by compression loading of rectangular-shaped samples [17]; however, the nature of the studies—single-point displacement of small fragments of tissue—limits the application to clinical conditions. In an effort to improve the physiological accuracy of ex corpus testing, some studies have perfused the excised organs (spleen [16], kidney, and liver [18]). In vivo skin biomechanical measurements have been obtained in research on prosthetics [19–21], using techniques that may be applicable to internal organs.

Several experimental devices have been specifically developed for acquiring biomechanical properties of soft tissues in vivo and in vitro under various loading conditions: tissue elongation [22], indentation (TeMpEST 1-D device [23] and another handheld device [15]), puncture forces (instrumented needle) [22], rotary shear (ROSA-2) [24], tissue grasping (instrumented grasper) [25,26], and tissue cutting (instrumented scissors) [27]. Building on this experience, our group has developed a series of devices for measurement of tool-tissue interactions during minimally invasive surgery: the Blue DRAGON system [28–30] and the force-reflecting endoscopic grasper (FREG) [31]. Based on data collected with the Blue DRAGON system, the motorized endoscopic grasper (MEG) was designed to reproduce the maximum grasping forces and velocities observed during surgical tissue manipulation and acquire more extensive and reliable compressive data from abdominal organs [32–34].

There is substantial literature on empirical mathematical models for the soft tissue response to various mechanical loading conditions. Many tissues follow an exponential relationship between stress and strain [2,17,22,31]. There are many approaches for modeling the time-dependent response of soft tissues, including quasilinear viscoelasticity (QLV) [2,35,36], biphasic models [37–43], and even triphasic theory [44] involving solid, fluid, and ionic concentration state variables. While there is much potential to apply high-order, multiaxial, time-dependent models to our collected data, the scope of the reported study is limited to fitting the collected force-displacement data to nominal uniaxial stress-strain and time-dependent exponential functions.

It is evident from the literature that four essentials are lacking for modeling tissues in the context of surgery: (1) a base line understanding of *how* surgeons interact with tissues (i.e., to establish the relevant scale of stress and strain), (2) *compression* testing, (3) *in vivo* data, and (4) *human* data. Typical biomechanical studies have tested tissues in vitro in tension using excised animal specimens (often after freezing and thawing). In this paper, we address the first three issues to provide a more complete understanding of the in vivo biomechanics of laparoscopic surgery. The selected stress and strain levels were based on measurements of forces, torques, and displacements applied by surgeons during training procedures in pigs. The focus on compression comes from the fact that most tissue manipulation during minimally invasive surgery (MIS) involves some form of grasping, and surgeons frequently squeeze or palpate tissues to find diseased areas, tumors, or lesions. Additional data will be presented to illustrate the changes between in vivo and in vitro properties. The aims of this paper are to (1) report compressive properties of several gastrointestinal (GI) organs relevant to laparoscopic surgery in vivo and ex corpus, (2) measure the same properties of these organs after death and with a traditional testing instrument, and (3) develop phenomenological models of the acquired data.

The experimental animal (pig), the instruments, organs, and surgical procedures were selected to be most relevant to the domain of general GI surgery. Organs of interest included bladder, gallbladder, liver, spleen, stomach, large intestine, and small intestine.

2 Methods

2.1 Definitions. In this study, in vivo will refer to testing done inside an intact live specimen, with the organ in its normal position. In situ will refer to testing the same organs after the animal has died, but with the organs still in the body proper. In vitro refers to testing done outside the body, using tissue samples that have been excised from the bulk organ. Finally, ex corpus will refer to intact, nonliving organs removed from the body, and possibly stored before testing some time postmortem.

2.2 Tools. Two types of tools were used to acquire the biomechanical properties of internal organs in vivo, in situ, and ex corpus: (1) a custom-made MEG, used in all conditions, and (2) a servohydraulic universal-testing material testing system by MTS Corporation (Eden Prairie, MN), used for testing tissue ex corpus only.

2.2.1 Motorized Endoscopic Grasper. The MEG is the second generation of FREG [31] that was originally designed as a one degree-of-freedom (DOF), bilateral teleoperated system, but was also capable of applying in vivo computer controlled sequences of compressive force via a flat-coil actuated endoscopic grasper (slave element). As such, it was used to test several porcine abdominal tissues in vivo to measure their stress-strain response but could only apply approximately 8 N compressive force that was estimated by measuring the current to the flat-coil actuator. Following these research efforts, the MEG was designed to further examine the compressive properties of porcine abdominal organs [32,33]. The engineering specifications of the MEG were based on data collected from previous experiments using the Blue DRAGON surgical tool tracking system [45]. These data were examined in order to determine the forces, deformations, and timing of compressive loads applied on tissues.

The MEG uses a brushed DC motor (RE25, 10 W, Maxon Precision Motors, Fall River, MA) with a 19:1 planetary gearhead (GP26, Maxon Precision Motors, Fall River, MA) to drive a Babcock grasper (No. 33510 BL, Karl Storz, Germany), Fig. 1. The gearhead output shaft is attached to a capstan that drives a cable and partial pulley. The pulley is attached to a cam joint that converts the rotational motion of the motor and pulley to a linear translation of the grasper shaft, which opens and closes the jaws. A 500 count digital encoder (HEDL55, Hewlett-Packard, Palo Alto, CA), attached to the motor, measures angular position. The mechanism's overall effective gearing ratio is approximately 190:1, including the planetary gearhead ratio (19:1) and the partial pulley-capstan gearing ratio (10:1), increasing the 29 mN m of continuous torque generated by the motor to 5.51 N m applied by the partial pulley. A wide variety of standard Karl Storz laparoscopic instruments can be attached to the base plate mount, but a Babcock grasper (Fig. 1(*c*)) was selected as the primary loading device due to its special geometry. Range of motion for the Babcock jaws is 54.3 deg, or 184 deg at the capstan. Resolution of jaw angle is approximately 1.13×10^{-2} deg per encoder count (5.5×10^{-3} mm at the jaws' grasping surfaces). At full opening, the two grasping surfaces are 26.3 mm apart.

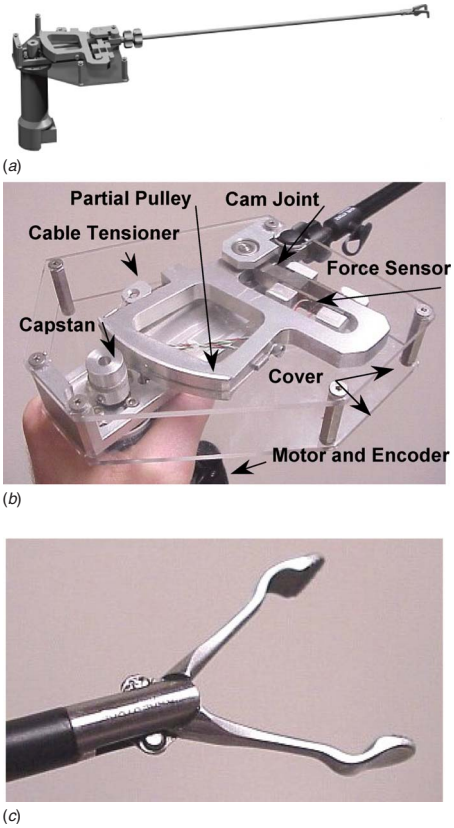

Fig. 1 The MEG: (*a*) rendered CAD drawing of MEG (protective top cover not shown), (*b*) close-up photograph of the MEG's drive mechanism, and (*c*) close-up photograph of the MEG's Babcock grasper end effector

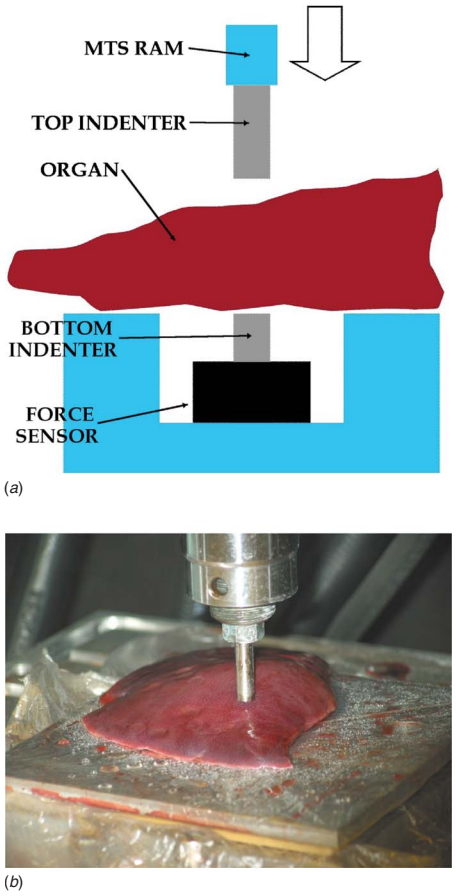

Fig. 2 MTS experimental testing machine setup: (*a*) schematic overview of the system and (*b*) the setup with a liver ex corpus

A double-beam planar force sensor (FR1010, 40 lb, Futek, Irvine, CA) is mounted in the partial pulley, measuring force applied to the end effector. The signals are amplified with a Futek signal conditioning unit (Model JM-2). The resolution of force signals following a 16 bit analog/digital (A/D) conversion is 0.6 mN. A noise level of up to 50 mN, including the quantization noise, was observed, which represents 0.025% of the sensor's full scale. The maximum continuous motor torque of 29 mN m is equivalent to 26.5 N of grasping force by the Babcock grasper's jaws, after transmission through the mechanism, which is greater than the average force applied by surgeons during typical surgical tasks [45]. Based on the Babcock grasper's jaw dimensions, the application of 26.5 N is equivalent to a compressive stress of 470 kPa. The MEG is handheld and weighs 0.7 kg. It is inserted into the body through standard 10 mm endoscopic "ports" used for passing videoendoscopic instruments into the body without losing the gas pressure in the abdomen.

Computer control of the MEG is provided via a personal computer (PC) using a proportional-derivative (PD) position controller implemented in SIMULINK (Mathworks, Natick, MA) and DSPACE (Novi, MI) user interface software (ControlDesk) and hardware (DS1102). Current is supplied to the motor via a voltage-controlled current supply (escap ELD-3503, Portescap, Hauppauge, NY) controlled by the output from the DSPACE board (D/A 16 bit). The control loop runs at 1 kHz. The MEG was calibrated to address the nonlinear relationship between the position of and the force applied by the distal tool tips with respect to the sensors located on the proximal end of the tool (defined analytically in Ref. [31]), as well as to compensate for mechanism compliance and backlash.

2.2.2 MTS Setup. The testing system by MTS Corporation is a standard servohydraulic universal-testing machine often used in material testing in the field of biomechanics. The custom-built frame was used with a Model 252 valve. A maximum closed-loop velocity of the ram using this valve is 500 mm/s.

The experimental setup used with the MTS machine for tissue testing is shown in Fig. 2. The top and bottom indenters were identical 7 mm diameter right circular cylinders providing a contact area of 38.5 mm^2, compared to the MEG's contact area of 56.4 mm^2. The top indenter is screwed into the MTS ram (the moving portion of the machine). The bottom indenter was fixed to the tension/compression force sensor (44.5 N tension/compression unit, Sensotec Model No. 31/1426-04). The force sensing resolution was 21.7 mN. A noise level of up to 9 mN including the quantization noise was observed, which represents 0.019% of the sensor's full scale. The force sensor rested in a stainless steel base plate that was affixed to the MTS frame. The top of the base plate and the top of the bottom indenter were aligned. The organ rested on the base plate and the bottom indenter. The opening was just large enough to accommodate the force sensor but not allow the tissue to droop significantly. Additionally, the base plate had two grooves, one vertical slot for routing the force sensor's wire and the other a horizontal one around the entire base for cinching down a very thin plastic sheet with a rubber band. This plastic sheet protected the force sensor from fluids present during testing. Despite the presence of this sheet and the fact that the effective top of the force sensor and the rest of the plate were level, it was assumed that the force sensor would measure the majority of the applied pressure, since the film was very thin and flexible and there was a relatively large gap surrounding the force sensor in-

denter (Fig. 2).

The MTS ram was operated in a position-control mode using TESTSTAR II software and hardware. Axial position was sensed using a linear variable displacement transducer (LVDT) mounted on the hydraulic ram in the frame's crosshead (Model 244.11). Analog signal conditioning was performed in hardware before passing to the PCI-based, 12 bit analog/digital conversion board (PCI-6071-E, National Instruments). The axial position resolution was 0.0074 mm in a preset ± 15.24 mm range. Data were sampled at 1 kHz or faster.

One may note that the sensors on the MTS and MEG aimed to measure the end effector position (and therefore the tissue thickness), and the forces applied on the tissue are located at different places along their respective kinematic chains, starting at the actuator and ending at the end effector. However, given the kinematics and the dynamics of each chain, the sensors' readings were mapped from their locations to the devices' end effectors. Locating the MEG's position and force sensors proximal to the end effector without altering the end effector itself was motivated by the desire to use standard surgical instruments in a typical surgical environment. Placing a sensor on the end effector that could survive the in vivo environment while not significantly altering the tool's geometry and/or ability to be used in vivo would be extremely difficult. Moreover, since the endoscopic tool remained unchanged, it is possible to completely remove it from the MEG, sterilize it, and use it in a survival procedure.

2.3 Experimental Protocol and Loading Conditions. Three-month-old female pigs (porcine Yorkshire cross) with an average weight of 37 (± 5) kg were used as the animal models for the experimental protocol. The same animal model is used for training laparoscopic surgeons due to its similar internal abdominal organ anatomy to humans. Seven internal organs (liver, spleen, bladder, gallbladder, small and large intestines, and stomach) taken from 14 different pigs were tested in various testing conditions (in vivo, in situ, and ex corpus). The MEG was used for testing all seven organs of six animals, whereas the MTS machine was used on four organs (liver, spleen, small intestine, and stomach) from three animals. The MEG was used in all conditions, while the MTS was obviously used for only ex corpus testing. (The remaining animals were tested with some mix of condition and organ.) The in vivo and in situ experiments were recorded visually using the endoscopic camera, synced with force-deformation data, and recorded on digital video for off-line analysis and archival.

In vivo tests were performed on a sedated and anesthetized animal as per standard veterinary protocols and typical for a laparoscopic training procedure at the University of Washington Center for Videoendoscopic Surgery, an AALAC-accredited facility. The abdomen was insufflated with CO_2 to a pressure of 11–12 mm Hg, as typical in porcine MIS procedures. Three laparoscopic ports (10 mm in diameter) were placed into the abdomen, which allowed access to all the organs to be tested as well as visualization of the tool tip by the endoscopic camera. In situ tests were conducted under the same experimental conditions on the euthanized animal immediately postmortem. Ex corpus testing was performed at the UW Applied Biomechanics Laboratory. For the organ harvesting, blood vessels to the organs were cut, and blood was free to drain and clot. Hollow organs were stapled and then cut to ensure that any contents remained intact. The organs were kept moist with 0.9% saline solution and stored in an ice chest with ice packs. The ex corpus testing took place in a climate-controlled room; the temperature was held at 22.7°C with a humidity of 22% during all the tests. During the ex corpus tests, the tissues were constantly kept moist with sprays of saline solution; the organs were never frozen.

Cyclic and step strains were used as the two loading conditions for testing the various soft tissues. In addition to these two loading conditions, the tissues were tested to failure, defined by a tissue fracture, by both devices ex corpus. The loading characteristics used as part of the experimental protocol were defined based on a detailed analysis of the grasping action in laparoscopic surgery, as measured by the Blue DRAGON system [45]. Moreover, since laparoscopy, by definition, is performed in vivo, collecting load-response data under similar conditions is paramount to reflecting the nature of these biological materials as clinically presented to the surgeon. Emulating surgical conditions as part of the experimental protocol guaranteed that models that were developed based on the collected data reflected the appropriate nature of these biomaterials for future applications, such as haptic virtual reality surgical simulators. This concept profoundly manifested itself in the experimental protocol design and execution.

One of the major deviations from a more common soft tissue biomechanical testing protocol was in regard to tissue preconditioning. Due to the viscous nature of soft tissues, their deformation response changes with each successive loading cycle [2]. A stable behavior can develop after several loading cycles, at which point the tissue has been "conditioned," and its hysteresis loop is minimized. Conditioning a tissue before testing (referred to as "preconditioning") often takes 10–20 cycles, depending on the tissue and the loading condition [2]. Since tissues are not preconditioned before being manipulated in surgery, first-cycle behavior is of great interest, as is steady-state behavior and the number of cycles to reach conditioning. No preconditioning was performed during this study. A new site (location on the organ) was used for each test regime to ensure that the natural (unconditioned) state of the tissue was measured.

Initial tissue thickness was determined by the distance between the tool tips (or indenters) at the point of the first contact. Each subsequent cycle used this same value, whether or not the tissue was actually in contact at this distance. This was done to observe any depressions left in the tissue after the previous compression.

The first type of load applied was a cyclic position (strain) wave form, in order to examine the tissues' elastic stress-strain response. The constant velocity (triangle-shaped) strain signal was the cyclic loading profile of choice for the following reasons: (1) it allows controlled strain rate, (2) it facilitates tool-tip contact detection based on deviation from nominal velocity, and (3) it has been used in previous studies. The second type of load applied was a single position (strain) step, in order to examine the stress-relaxation properties of the tissues. A viscous material exhibits an exponential decrease in the measured stress within the material while the strain is held constant. Analysis of measurements made with the Blue DRAGON [45] indicated that the maximum grasp time during various surgical tasks was 66.27 s. The average maximum grasp time was 13.37 ± 11.42 s, the mean grasp time was 2.29 ± 1.65 s, and 95% of each subject's grasps were held for less than 8.86 ± 7.06 s. Based on these results, a short hold time (10 s or less) could be used for loading the tissues. However, it is useful for modeling purposes to examine the relaxation over a longer period of time, in order to better characterize the behavior. For practical purposes, the step strain was held for 60 s at three different strain levels (in different tests), targeted between 42% and 60% strain. During the step strain tests, the MEG end effector was commanded to close as rapidly as mechanically possible. It is important to note that the entire organ under study remained intact throughout the experimental protocol. Although the compressive loads were uniaxially applied on the various organs, the surrounding tissues of the organs themselves define the boundary conditions. These boundary conditions are fundamentally different from the boundary conditions of a sample of tissue removed (excised) from an organ. With such a sample, either free boundary conditions or confined boundary conditions within a fixed geometry can be used. Setting such controlled boundary conditions is a common practice in material testing; however, keeping the organ intact better reflects the boundary conditions encountered during real surgery. These testing conditions imply that the results reported in this study refer to both structural and material properties of tis-

sues, not just to the material properties. The testing locations on the organs were limited to the organs' peripheries for both the MEG and the MTS. These testing locations were selected due to the fact that the Babcock jaws of the MEG were less than 3 cm long; it was impossible to test the interior bulk of the larger organs like liver and stomach with the MEG.

2.4 Data Analysis: Phenomenological Models. Two fundamental approaches exist for developing models of soft tissue mechanical behavior: (1) constitutive, physical law-based models, such as strain energy function models, and (2) phenomenological models based on curve-fitting experimental data. The former approach leads to easier extraction of physical meaning of the parameters but may not have perfect fits with the acquired data. The latter approach has little or no physical relevance but may achieve excellent fits to the acquired data with potentially less computationally intensive functions. Due to the empirical emphasis of this study, a phenomenological modeling approach was used. In order to evaluate which of these methods should be selected, a series of candidate curves were defined and evaluated for their ability to accurately and consistently fit a significant portion of the dataset. The measures of fit that were examined were the mean, median, and standard deviation of both regression coefficient (R^2) and root mean squared error (RMSE).

2.4.1 Elastic Models. Eight functions were chosen to model the elastic characteristics of the tissue. In these equations, the engineering (nominal) stress (σ) is defined to be the ratio of compression force (F) applied on the tissue to the contact area (A), Eq. (1*a*). The engineering strain (ε) is defined as the difference between the initial thickness of the tissue (l_0) under no load and the actual thickness under the compression load (l) normalized with respect to the initial thickness, Eq. (1*b*). Each model assumes zero compressive stress (σ) at zero strain (ε), and a positive stress at positive strain. Theoretically, compressive strain must be less than unity (1), since a value of 1.0 indicates that the material has been totally compressed.

$$\sigma = \frac{F}{A} \tag{1a}$$

$$\varepsilon = \frac{l_0 - l}{l_0} \tag{1b}$$

The first function (Eq. (2)) to be examined is a basic exponential function, referred to as EXP. Various forms of this equation have been used by several researchers [2,15,18,22,31]. α and β are coefficients determined by curve fitting the experimental data.

$$\sigma = \beta(e^{\alpha\epsilon} - 1) \tag{2}$$

The second function (Eq. (3)) is an expansion of EXP, introducing a linear term and increasing the order of strain to ε^2. This equation was developed for this study and is referred to as EXP2. Again, γ is a coefficient obtained by curve-fitting the experimental data.

$$\sigma = \beta(e^{\alpha\epsilon^2} - 1) + \gamma\epsilon \tag{3}$$

The third function (Eq. (4)) incorporates the inverse of strain and is referred to as INV. This equation introduces a vertical asymptote in the stress-strain relation. This asymptote must lie between $\varepsilon=0$ and $\varepsilon=1$. There may be some physical relevance to the value of this strain asymptote: it may reflect the amount of fluid within the tissue that cannot be exuded, or the point at which the tissue becomes incompressible.

$$\sigma = \beta\left(\frac{1}{1 - \alpha\epsilon} - 1\right) \tag{4}$$

The fourth function (Eq. (5)) is a uniaxial form of a Blatz–Ko model and is referred to as BLATZ. This equation was previously used to model the kidney and liver under compression loading [46].

$$\sigma = \frac{-\gamma}{\alpha + 1}\left((1 - \epsilon)e^{\alpha((1-\epsilon)^2 - 1)} - \frac{1}{(1 - \epsilon)^2}e^{\alpha(1/1-\epsilon - 1)}\right) \tag{5}$$

The final functions (described by Eq. (6)) are polynomials with increasing order from second ($i=2$) to fifth ($i=5$). They are referred to as POLY2 through POLY5.

$$\sigma = \sum_{i=1}^{n} c_i \varepsilon^i \tag{6}$$

The derivative of a stress-strain function with respect to strain defines the material stiffness, or tangent modulus. A linearly elastic material's stiffness would be a constant, or Young's modulus. The derivative of an exponential stress-strain relationship is a function of its strain (e.g., the derivative of Eq. (3) with respect to strain results in Eq. (7)). The "overall stiffness indicators" defined for EXP2 are $\beta\alpha$ and $\beta\alpha+\gamma$, which serve as useful scalars for roughly approximating overall stiffness of a material and allowing quick comparisons between materials.

$$\frac{d\sigma}{d\epsilon} = 2\alpha(\beta e^{\alpha\epsilon^2})\epsilon + \gamma \tag{7}$$

2.4.2 Stress-Relaxation Model. Three functions were selected to model the stress-relaxation data. The first function (Eq. (8)) is a logarithmic function with two time constants [2,15] that is referred to as RLOG:

$$\sigma(t) = -A\ln(t) + B \tag{8}$$

where

$$A = \frac{c}{1 + c\ln(\tau_2) - c\ln(\tau_1)}$$

$$B = A\left(\frac{1}{c} - \gamma + \ln(\tau_2)\right)$$

and γ is the Euler constant (γ=0.5772). Curve-fitting experimental data results in τ_1 and τ_2 (time constants) and c.

The second stress-relaxation function (Eq. (9)) is a decaying exponential function with a single time constant [2,20,47,48] that is referred to as REXP1:

$$\sigma(t) = 1 - a + ae^{-t/\tau} \tag{9}$$

with a being a curve-fit coefficient.

The third equation (Eq. (10)) is a decaying exponential raised to a power, with a single time constant. This function is referred to as REXP2.

$$\sigma(t) = \exp\left(\left(\frac{-t}{\tau}\right)^{\beta}\right) \tag{10}$$

3 Results

3.1 Elastic Testing. Example compression stress-strain experimental data plots of various internal organs are depicted in Fig. 3, and the associated elastic phenomenological model (EXP, EXP2, and INV) curve fits are plotted in Fig. 4. Example organ response data, as well as the phenomenological models and their fit are plotted for the liver in Fig. 5. The averages of the individual EXP2 model parameters across all conditions based on the MEG and MTS measurements in vivo and ex corpus are summarized in Table 2.

As indicated in Fig. 3, there is a major change in the stress-strain curve between the first and fifth loading cycles. Moreover, Fig. 3 depicts the spectrum of stress-strain characteristics bounded by the two extreme experimental conditions: (1) first-cycle compression in vivo—a typical loading condition during surgery (Fig.

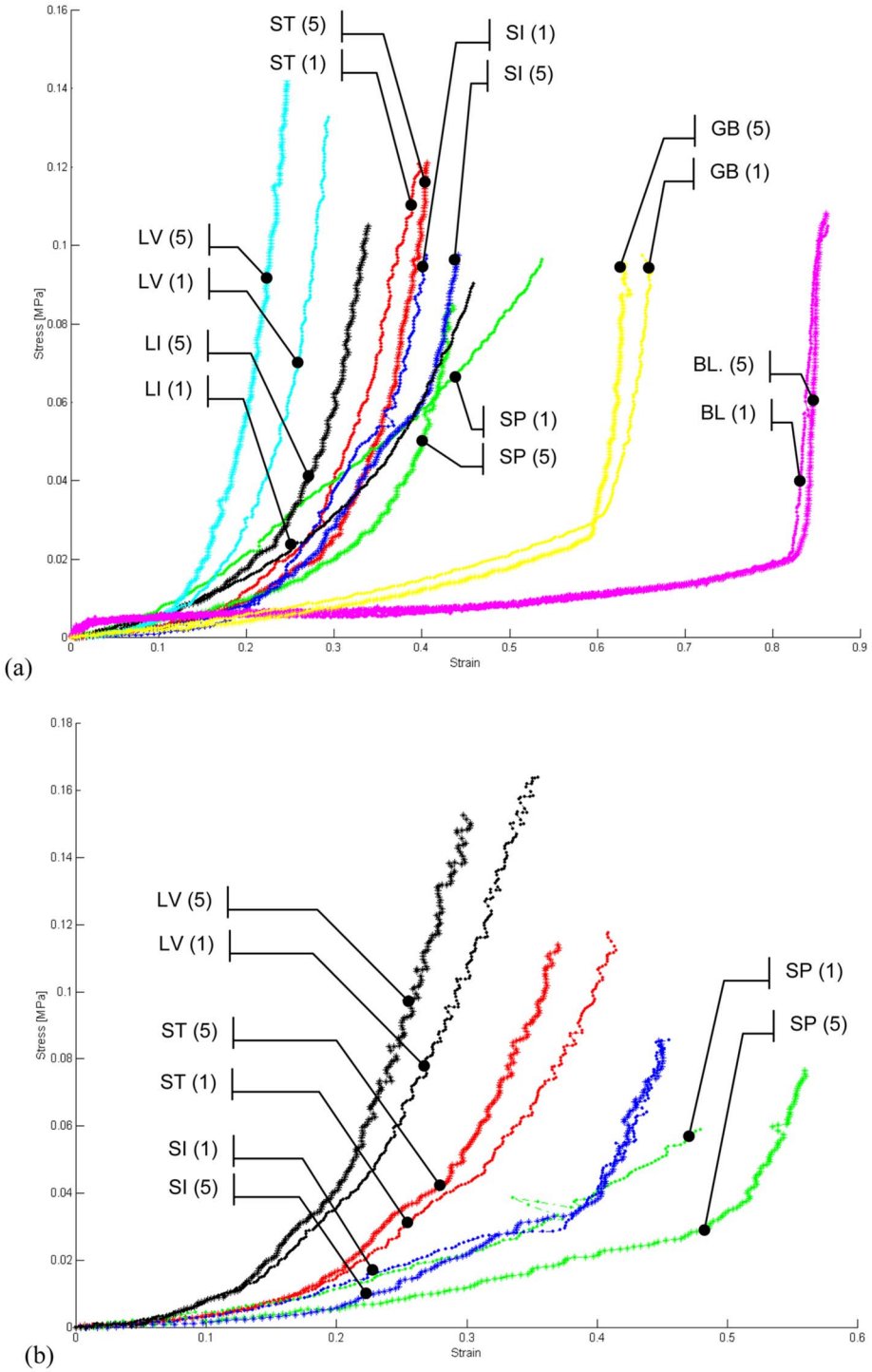

Fig. 3 Example stress-strain curves for all organs under study, as measured with the MEG at 5.4 mm/s loading velocity (first and fifth cycles shown): (*a*) in vivo and (*b*) ex corpus. Organs' legends: BL=bladder, GB=gallbladder, LI=large intestine, LV=liver, SI=small intestine, SP =spleen, and ST=stomach. The loading cycle number (1 or 5) is defined in the brackets.

3(*a*)), and (2) near-preconditioned fifth compression cycle ex corpus—a loading condition more typical to biomechanical characterization analysis of soft tissue (Fig. 3(*b*)).

In general, it appeared that a tissue's stiffness increased with subsequent loading cycles for the first seven to ten loading cycles, at which point the stress-strain behavior reached a steady-state phase, indicating the point at which the tissue likely became conditioned. Note the marked difference in shape of the stress-strain curve between first and fifth loading cycles in spleen (Figs. 3 and 4). This behavior was visually noted during spleen testing by the fact that the MEG jaws tended to leave a deep impression in the organ after the first loading cycle; the tissue did not recover to its initial thickness after the first loading cycle. The spleen also appeared to have a nearly constant stiffness on first compression but became more exponential on subsequent cycles. The hollow organs, particularly small intestine, tended to have two distinct parts

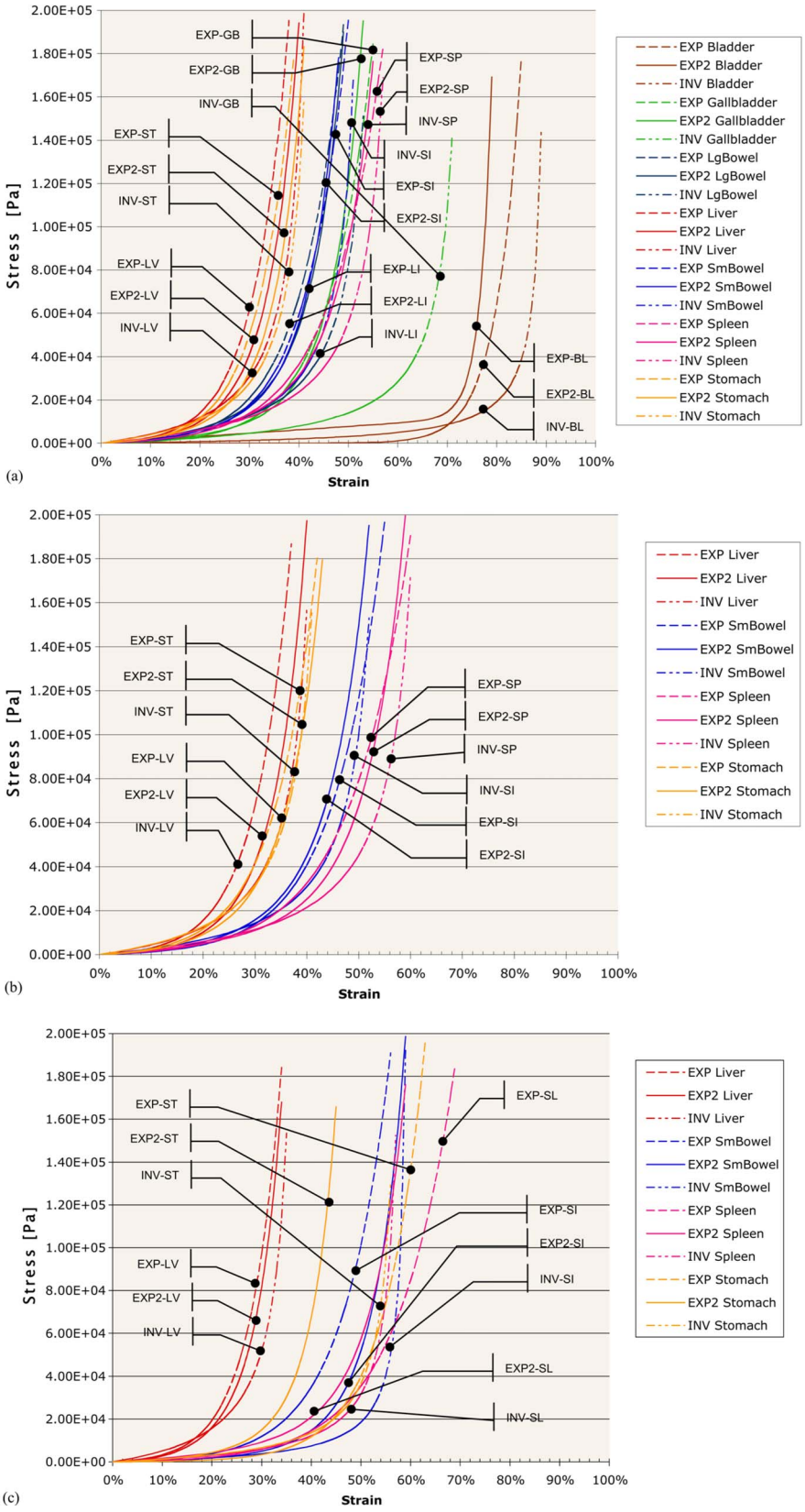

Fig. 4 Stress-strain curves for all organs with average curve-fit parameters across all conditions: (*a*) in vivo data measured by the MEG, (*b*) ex corpus data measured by the MEG and (*c*) ex corpus data measured by the MTS. Organ legend: BL=bladder, GB =gallbladder, LI=large intestine, LV=liver, SI=small intestine, SP=spleen, and ST =stomach. See text for the definitions of the functions EXP, EXP2, and INV.

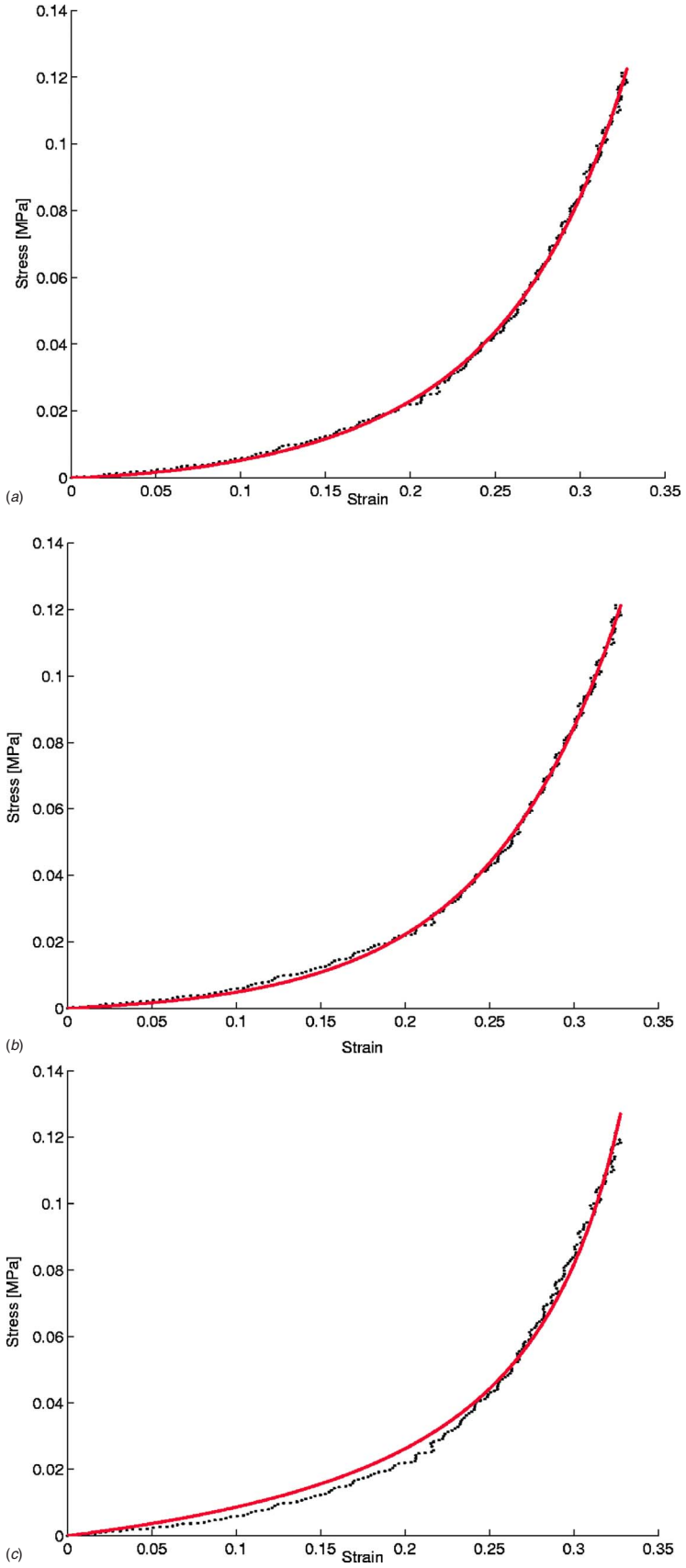

Fig. 5 Measured data and phenomenological models of liver tissue under compression loading. The same in vivo data measured by the MEG were fitted with various models. The measures of fit for these models are (*a*) EXP2, $R^2=0.9989$, RMSE$=1.5048\times10^3$; (*b*) EXP, $R^2=0.9984$, RMSE$=1.5166\times10^3$; (*c*) INV, $R^2=0.9931$, RMSE$=3.0291\times10^3$.

Table 2 Mean values of the EXP2 model parameters (β, α, γ) for each organ, in vivo and ex corpus, as tested by the MEG and MTS, across all animals, loading velocities, and cycle number

Device	MEG			MEG			MTS		
Condition	In vivo			Ex corpus			Ex corpus		
Parameters Organ	β (Pa)	α	γ (Pa)	β (Pa)	α	γ (Pa)	β (Pa)	α	γ (Pa)
Bladder	0.0041	27.98	15,439.2	N/A	N/A	N/A	N/A	N/A	N/A
Gall bladder	2304.5	15.75	9622.2	N/A	N/A	N/A	N/A	N/A	N/A
Large intestine	3849.7	16.14	16,544.1	N/A	N/A	N/A	N/A	N/A	N/A
Liver	7377.1	20.63	3289.4	7972.1	20.29	781.0	8449.8	26.26	1679.4
Small intestine	3857.3	16.60	11,273.8	6166.5	12.81	7967.5	1745.9	13.60	2,580.9
Spleen	3364.4	12.94	19,853.1	3798.8	11.31	14,440.4	2764.9	11.85	13,103.8
Stomach	4934.9	21.51	11,105.9	8107.0	16.91	6483.8	2247.6	21.22	6803.3

to their stress-strain curves, separated by an abrupt change in stiffness. The first part represents moving of the walls and compression of the contents (solid, air, or liquid). The second part occurs when the two walls of the organ contact each other. This portion can then be considered the actual deformation behavior of the *tissue* and should appear similar to the responses obtained by the other (solid) organs. One could argue that the entire curve represents the clinically relevant behavior of the *organ*.

Large intestine response to loading was different than the small intestine, which could be attributed to its thicker walls and generally larger shape (Fig. 3(*a*)). However, because it contained stool, it drastically tended to show different biomechanical behaviors between the first and subsequent squeezes as the contents were compressed and moved about. Small intestine tended not to have as much volume of contents as did the large intestine.

Two other hollow organs that show different behaviors from the other organs, bladder and gallbladder, were fluid filled. Therefore, their initial response was simply from the stretching of the membranous walls—more likely tensile testing than compression. When the walls finally came together, because they were so thin, the jaws were essentially touching and the sudden change in stiffness to nearly rigid was observed (Fig. 3(*a*)).

Ex corpus trends were generally similar to those seen in vivo (Fig. 3(*b*)). For example, small intestine still had the two-part shape, and the first-load cycle of spleen tended to be different from subsequent cycles. Ranges of stress and strain appeared to be similar as well. One key difference was the amount of internal compression variability. Aside from the difference between first and second loading cycles, the stress-strain behavior reached a consistent response more quickly. This may indicate a more rapid onset of tissue conditioning, or it could be less influence from in vivo factors such as ventilator motion and tissue reperfusion.

3.2 Stress-Relaxation Testing. Experimental data of normalized stress relaxation under compression loading are depicted in Fig. 6(*a*) for the liver. The stress was normalized with respect to the maximal value of the stress that was applied during the loading phase. The associated phenomenological models (REXP1, REXP2, and RLOG) and curve-fit functions are plotted in Figs. 6(*b*) and 7. The averages of the individual REXP2 (the overall best fitting model) parameters across all conditions based on MEG and MTS measurements in vivo and ex corpus are summarized in Table 3.

Example stress-relaxation data acquired from liver in vivo and ex corpus for various step strain levels are depicted in Fig. 6. The maximum value of the total decrease in stress (for this sample) was about 4–6% over the 60 s test in vivo, while the in situ and ex corpus maximum total decreases were 6% and 14%. The data indicate three general trends: (1) greater percent decreases in stress in the in situ and postmortem conditions compared to the in vivo condition, (2) greater decrease in normalized stress with less applied strain, and (3) greater decrease in normalized stress with increasing time postmortem (in situ versus ex corpus).

3.3 Failure: Liver. One benefit of testing tissues postmortem is the ability to test them to failure. Failure for liver tissue was examined for MEG and MTS tests (Fig. 8). Tissue failure is indicated in Fig. 8 by an abrupt decrease in stress. Liver failed at 35–60% strain with the MEG and 30–43% strain with the MTS at stresses of 160–280 kPa and 220–420 kPa, respectively. These results favorably compare with previously collected data reporting ultimate strain for liver at $43.8\% \pm 4.0\%$ (range: 39.0–49.1%) and an ultimate stress of 162.5 ± 27.5 kPa (range: 127.1–192.7 kPa), when loaded at 5 mm/s [17]. It is important to mention the difference in the boundary conditions between the two studies: in the study by Tamura et al. [17], rectangular samples were used rather than intact organs, as in this study. Some differences are therefore to be expected, but the orders of magnitude are similar, suggesting good agreement for both MEG and MTS results.

It was observed that failure mode was different for the MEG and MTS devices. The MEG, with its rounded and smooth jaw edges, tended to crush the internal structure of the liver, the parenchyma, a condition known as liver fracture. No damage to the outer capsule was visible, other than a depression. The indenter on the MTS machine, however, tended to tear the capsule before fracturing. This was likely due to the indenter's sharp edges and the sloping of the organ surface (Fig. 2).

3.4 Phenomenological Model Fit. Ranking the phenomenological models based on measures of fit (mean, median, and standard deviation of both R^2 and RMSE) separately and summing the ranks identified the best fitting model for each organ, as summarized in Table 1. The phenomenological model parameters were identified for each set of acquired data (per organ, testing condition, cycle number, etc.). One may note that the hollow organs appeared to be fit best by REXP2, while the solid organs were fitted best by RLOG.

3.5 Statistical Analysis of Phenomenological Model Parameters. One analysis of variance (ANOVA) was performed for each factor-measure combination, with a probability value of 95% (α=0.05). In Figs. 9 and 10, each measure is plotted against the levels for each factor (such as organ or compression cycle). The diamonds represent the mean for a given level (e.g., liver is a level of the factor organ), and the horizontal bars indicate the standard deviation. The black dots are the individual data points. The right-hand side of the plots depict the results from posthoc Tukey–Kramer honestly significant difference (HSD) analysis, as performed in the statistical software JMP (Cary, NC). This statistical test finds which pairs of levels have significantly different

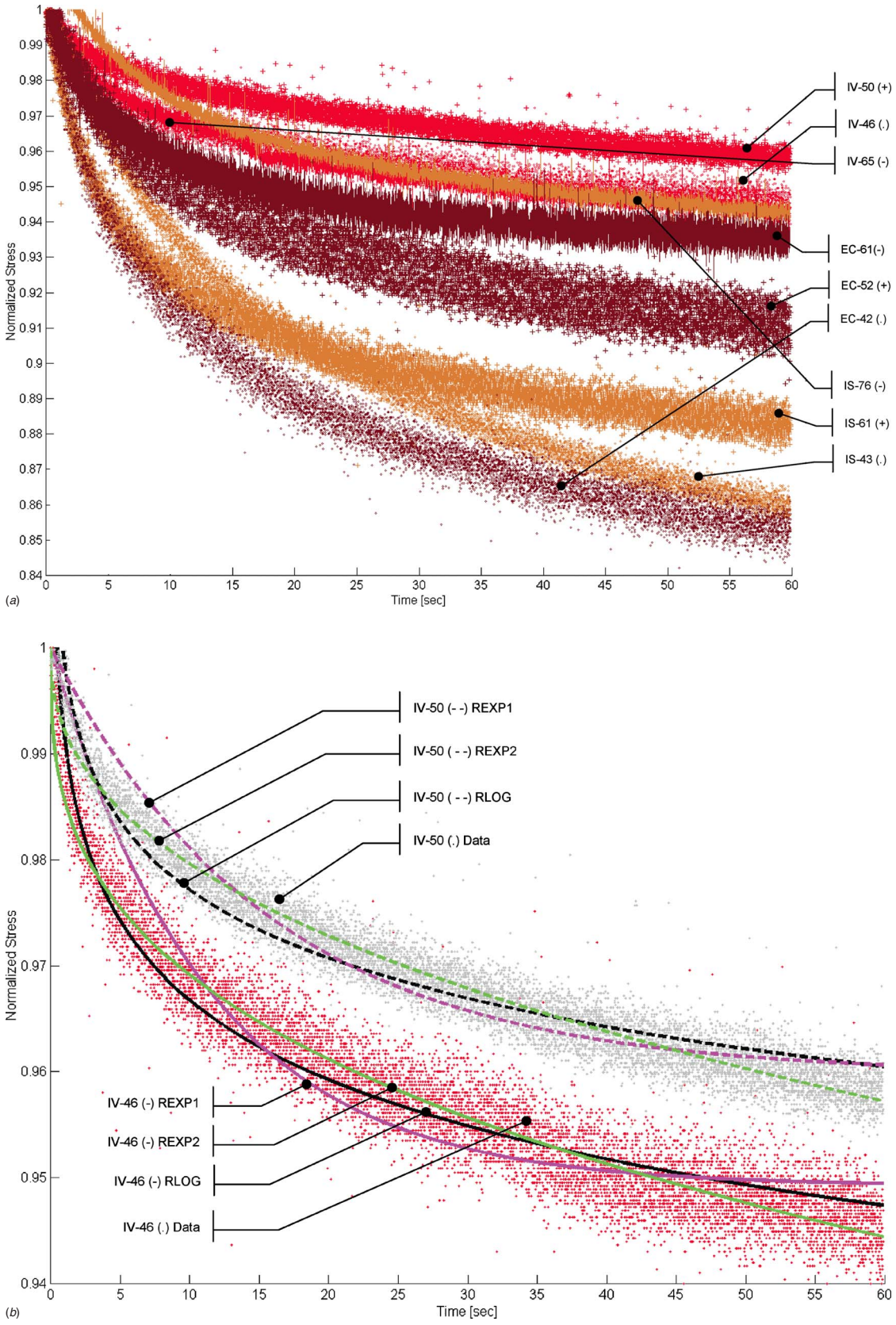

Fig. 6 Normalized stress-relaxation curves as a function of time for one liver tested with the MEG: (*a*) three different testing conditions (IV=in vivo, IS=in situ, and EC=ex corpus) and strain levels (indicated in the legends as a two-digit numeral (% strain); (*b*) measured data and phenomenological models of two strain levels. Their measures of fit: 46% strain (REXP1 (R^2=0.8948, RMSE=0.0042), REXP2 (R^2=0.9261, RMSE =0.0030), RLOG (R^2=0.9084, RMSE=0.0034)), and strain 50% (REXP1 (R^2=0.9387, RMSE=0.0026), REXP2 (R^2 =0.9526, RMSE=0.0021), RLOG (R^2=.9140, RMSE=0.0028))

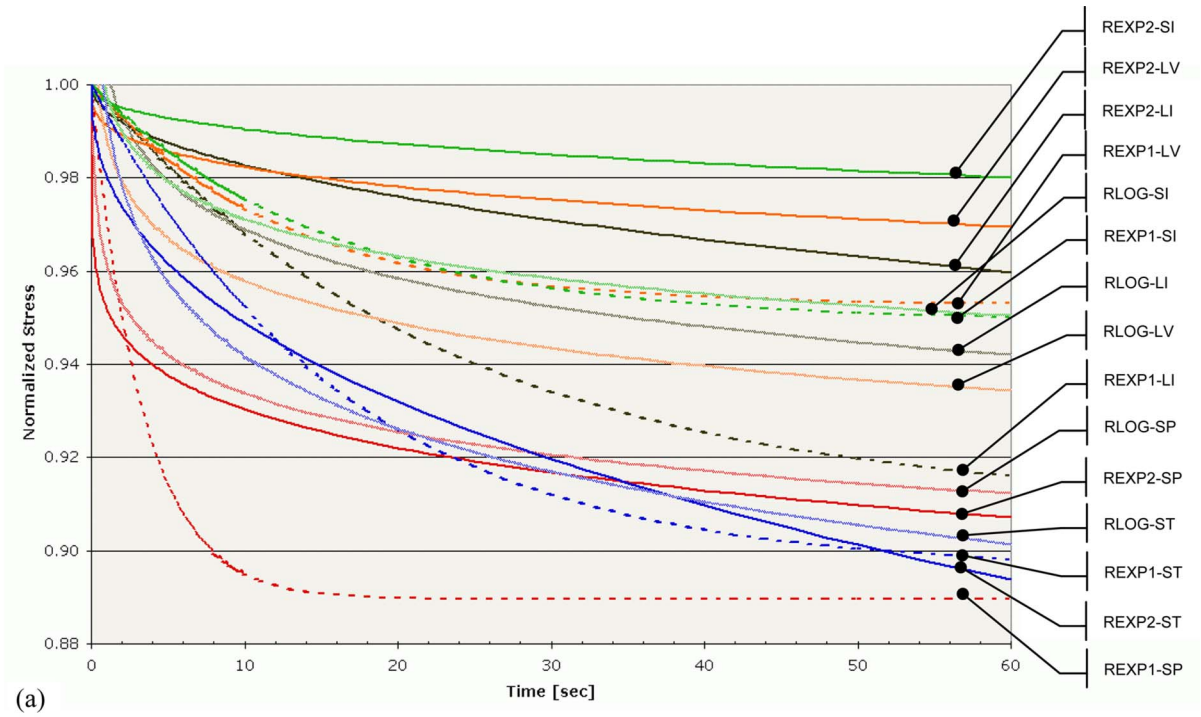

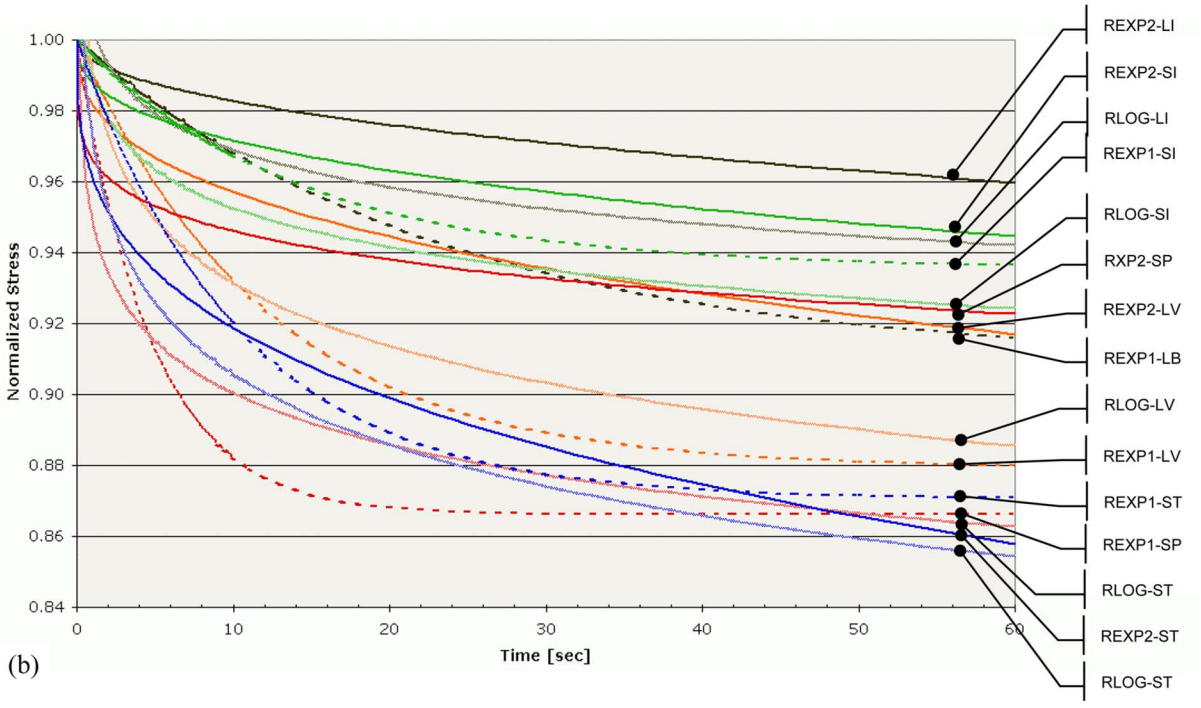

Fig. 7 Average normalized stress-relaxation curves for internal organs, based on mean values of REXP1, REXP2, and RLOG models: (*a*) in vivo and (*b*) ex corpus. Organ legend: BL=bladder, GB=gallbladder, LI= large intestine, LV=liver, SI=small intestine, SP=spleen, and ST=stomach. See text for the definitions of the functions REXP1, REXP2, and RLOG.

means, which is graphically represented by the circles: the center of each circle lies at the mean with the radius of the circle encompassing the region of confidence. If two circles overlap, then their means may not be significantly different and vice versa. The circles simply serve as a means for rapidly visually identifying significantly different groups.

Using the general stiffness indicator scalar $\beta\alpha+\gamma$ derived from Eq. (7) as a single indicator of the phenomenological model, a significant difference ($p<0.0001$) was found between the organs, indicating a significant difference in "stiffness" between most of the organs. Only 4 of the possible 21 organ pairs were not found

Table 3 Mean values of the REXP2 model parameters (τ, β) for each organ, in vivo and ex corpus, as tested by the MEG and MTS across all animals, loading velocities, and cycle number

Device	MEG		MEG		MTS	
Condition	In vivo		Ex corpus		Ex corpus	
Parameter / Organ	τ (s)	β	τ (s)	β	τ (s)	β
Large intestine	4.72*E*+04	0.479	N/A	N/A	N/A	N/A
Liver	4.95*E*+06	0.307	3.71*E*+04	0.381	1.40*E*+00	0.233
Small intestine	7.87*E*+05	0.412	1.13*E*+05	0.380	N/A	N/A
Spleen	6.70*E*+07	0.167	1.10*E*+07	0.208	8.84*E*−01	0.188
Stomach	1.03*E*+04	0.425	1.73*E*+04	0.331	4.59*E*−01	0.189

to be significantly different: spleen and small intestine, spleen and large intestine, small intestine and large intestine, and bladder and gallbladder (Fig. 9).

It is interesting to note that small and large intestines were not significantly different from each other using the overall stiffness measure ($\beta\alpha+\gamma$). Only when solely looking at the γ term does one find a significant difference. This would indicate that the overall behavior of the intestines is similar, especially at higher strains, but their behavior is significantly different at low strains.

There was a significant difference ($p<0.0001$) found between loading cycle with respect to stiffness indicator scalar $\beta\alpha+\gamma$ (Fig. 10). The stiffness indicator scalar for the first loading cycle was significantly greater than the seventh loading cycle and cycles 9–20. Moreover, the stiffness indicator scalar of the 2nd loading cycle was greater than that from the 13th, 16th, 17th, and 19th loading cycles. These results indicate that the stiffness indicator scalar in the first six loading cycles is generally larger than the latter loading cycles. A stable condition appears to be reached after seven to nine loading cycles.

Statistical analysis of the models' parameters indicated several significant differences as the function of the testing conditions (in vivo, in situ, and ex corpus). Tissue thickness at the beginning of each cycle (L_0) decreased significantly postmortem, which could be a result of lack of perfusion or from a breakdown in the tissue's structure. Tissues also tended to show greater inter-squeeze variability in vivo compared to postmortem. This could have been due simply to noise or motion artifacts during the in vivo testing. The elastic EXP2 parameters alpha and gamma both decreased significantly with time postmortem, and the overall stiffness of the tissues appeared to be less stiff than in the in vivo condition (see Fig. 4). The relaxation tests yielded few statistically significant results, but general trends were observed, most notably that the amount of relaxation in the tissues appeared to be greater postmortem than in vivo.

There were significant differences in the results from MEG and MTS machines, which could indicate inaccuracy in one or both testing devices, but the more likely cause is the slightly different loading conditions applied in the two setups.

4 Conclusions and Discussion

Structural biomechanical properties (stress-strain and stress relaxation) of seven abdominal organs (bladder, gallbladder, large and small intestines, liver, spleen, and stomach) have been obtained using a porcine animal model. The organs were tested in vivo, in situ, and ex corpus under compressive loadings using a novel device, the MEG, and a standard universal material testing system (MTS). The tissues were tested with the same loading conditions commonly applied by surgeons during minimally invasive surgical procedures. Phenomenological models were developed for the various organs, testing conditions, and experimental devices. The results indicate significant quantitative differences between tissue properties measured in vivo and postmortem conditions that will be of value for developing performance criteria for the next generation of surgical robots and simulators.

One of the most difficult aspects of any testing of biological materials is the large degree of variability (difference between animals, heterogeneity of the organs, strain history dependence, strain rate dependence, etc.). This particular study compounded this problem by testing bulk organs in vivo and without preconditioning. Testing tissues in vitro, using specimens of known shape under very controlled loading and boundary conditions, can usually lead to results with lower variability, particularly if the tissues are preconditioned. Testing in vivo also introduces potential sources of noise, such as movement artifacts from beating heart and respiration, varying rates of tissue reperfusion, etc. Unfortunately, this variability may mask effects from other factors. Some of this might have been quantified by repeated testing of the same site, but the fact that the tissues exhibit strain history dependence makes this impractical: the sites would have to be allowed to fully recover to their natural state before subsequent testing, requiring the animal to be anesthetized for extended amounts of time. While this variability makes finding statistical significance in the data difficult, for the scope of surgical simulation, it is worthwhile to determine ranges of tissue properties.

With this information, simulators can realistically change the organs' virtual mechanical behavior so that the virtual liver operated on in one session would be different from the next. Providing realistic force magnitudes identical to those felt by surgeons when grasping organs during actual surgery is the first step toward more realistic and scientifically based surgical simulators incorporating haptic feedback. In addition, surgical instruments and surgical robot manufacturers can use this information for optimizing their products to provide sufficient grasping traction while minimizing trauma. This could decrease costs and improve patient outcome.

The goodness of fit measures of the phenomenological models to the experimental data is based on residual error. In the case of the elastic tests, the residual error is typically highest at large strains, where small changes in strain cause rapid increases in stress. Therefore, the best fitting curves are often the ones that fit best in the large strain region (the steepest part of the curve) but may or may not fit as well at lower strains. The study of the stress-strain database shows that nearly any set of data can be fitted well by a sufficiently high-order equation. However, this becomes unwieldy and physically irrelevant. Due to the large number of parameters in POLY4 and POLY5 and the fact that the functions are not monotonically increasing, these models are not the model of choice for internal organ soft tissues, despite their good measures of fit. Moreover, the functions POLY2 and POLY3 and BLATZ lacked sufficient goodness of fit. The INV and EXP2 models provided better results than EXP, which is a curve commonly used in soft tissue studies. The EXP model may be better suited for tensile experiments, where there is no vertical asymptote before failure. Due to the nature of compression, strain varies from 0 to 1 and can never reach unity (1). For bulk materials that have not failed, there will always be a strain asymptote between 0 and 1. INV explicitly provides this number by its β term: the asymptote occurs at $\varepsilon=1/\beta$. This may shed some physical insight into the nature of the tissues. Perhaps, this value of β represents the thickness of the fluid within the tissue that cannot be exuded, thus leading to an incompressible state. While EXP2 does not provide this physical information and has three parameters instead of two, it overwhelmingly is the best fitting of all the exponential-type functions and the best fitting of all functions under study.

Fitting models to stress-relaxation tests is highly dependent on the duration of the test. Extrapolation beyond the testing period may lead to inaccurate results. Only the REXP1 model, of the three models examined, has a stress asymptote (of value $1-a$), which is usually what is observed in tissue. Soft tissues are generally considered viscoelastic, which means that there is some elastic component and a viscous component. After infinite time in

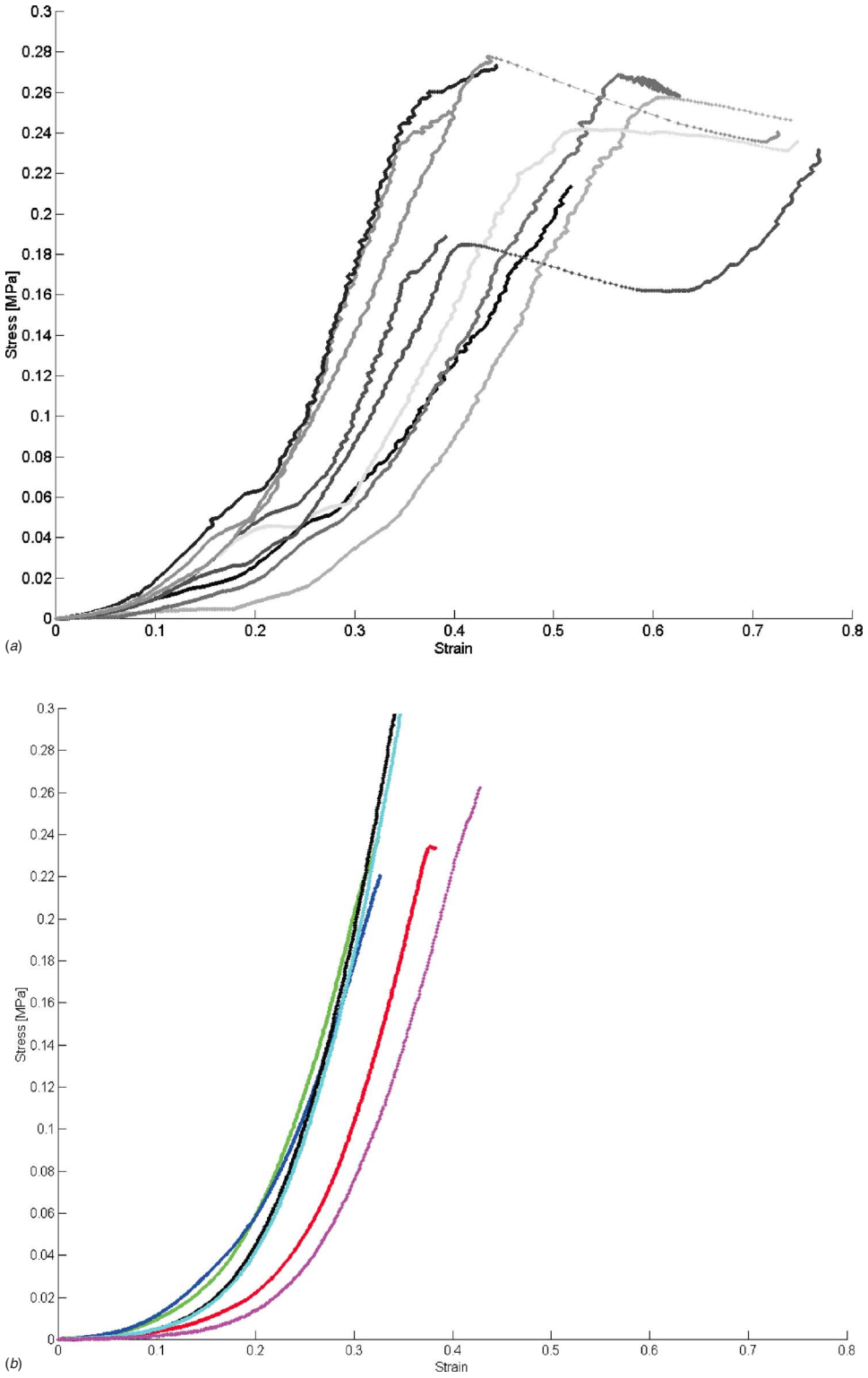

Fig. 8 Ex corpus stress-strain characteristics of the liver under compression loading to failure: (*a*) MEG, (*b*) MTS

compression, little stress is developed in the viscous component, and only the elastic component will remain, which is a finite, nonzero value. Models such as REXP2 and RLOG lack the asymptotic behavior as contained in REXP1. Therefore, extrapolating data based on these two models may predict nonphysical behavior in which the stress continually decreases as a function of time, even beyond a value of zero—a physical impossibility. Despite this, REXP2 was overwhelmingly the best fit model to these data, for the given test conditions.

Analyzing the models' parameters of all the tissues under study that were tested with the MEG across the various conditions (in vivo, in situ, and ex corpus) indicated the following characteris-

Table 1 The best fit of phenomenological models to the in vivo experimental data acquired from various internal organs by the MEG under the two compression loading conditions (elastic stress-strain and stress relaxation) across all conditions. Models in parentheses are based on data acquired by the MTS system (ex corpus only).

Organ	Data type	Model
Bladder	Elastic	EXP2
Gallbladder	Elastic	INV
Large intestine	Elastic	EXP2
	Relaxation	REXP2
Liver	Elastic	EXP2
	Relaxation	RLOG (REXP2)
Small intestine	Elastic	EXP2
	Relaxation	REXP2
Spleen	Elastic	EXP2
	Relaxation	RLOG (REXP2)
Stomach	Elastic	EXP2
	Relaxation	REXP2 (REXP2)

tics. Given the elastic model EXP2 (Eqs. (3) and (7)), the parameter γ significantly decreased ($p<0.0068$) as a function of the time postmortem. The parameter γ represents the more linear portion of the stress-strain curve, which dominates the stresses generated at low strains. Therefore, the results indicate that lower stresses were developed for small strains postmortem as opposed to in vivo. The stiffness indicators $\beta\alpha$ and $\beta\alpha+\gamma$ were significantly increasing ($p<0.0001$) as a function of the time postmortem. The results of the stress-relaxation tests indicated that the tissue recovery between successive periodic step strains was greater for longer rest periods and for in vivo. These phenomena can be explained in part by the higher perfusion of pressurized fluids within the tissues in vivo, the lack of which may contribute to the greater relaxation of the tissue postmortem than in vivo.

Despite the variability in the data, this study is a first step toward characterizing the highly complex behavior of abdominal soft tissues in their in vivo state. The MEG is a useful and effective device capable of measuring compressive structural properties of abdominal tissues under in vivo and surgically realistic conditions.

A full experimental characterization of a nonlinear, fluid-perfused, nonisotropic material such as the major internal organs in vivo is a complex endeavor. Proper modeling of bulk materials requires knowledge from triaxial testing that can only come from tissue biomechanical studies that are not similar to surgical conditions. The aim of this experimental protocol is to characterize

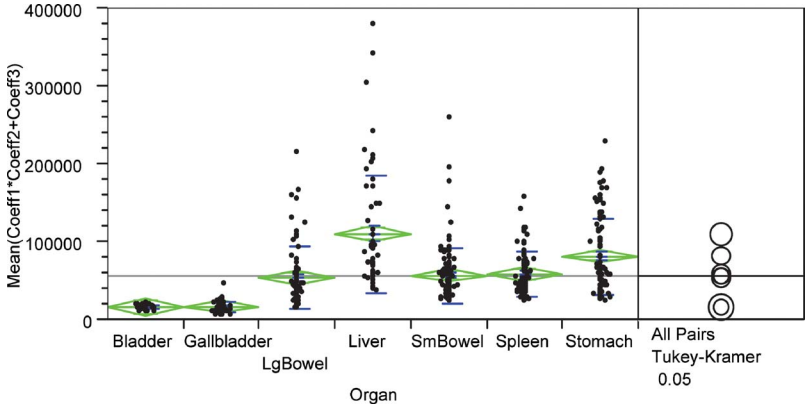

Fig. 9 The stiffness indicator scalar $\beta\alpha+\gamma$ of the EXP2 phenomenological model plotted for various organs for measured elastic data. The right-hand side of the plot depicts the results from posthoc Tukey–Kramer HSD analysis. The radius of the circle represents the region of confidence (95%).

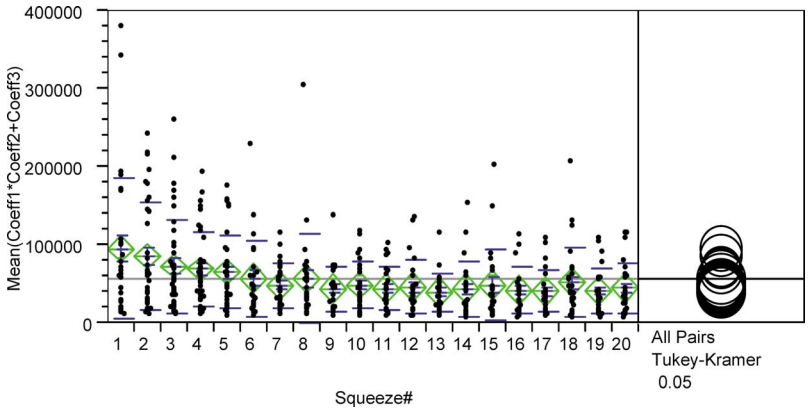

Fig. 10 The stiffness indicator scalar $\beta\alpha+\gamma$ of the EXP2 phenomenological model plotted as a function of loading cycle for measured elastic data. The right-hand side of the plot depicts the results from posthoc Tukey–Kramer HSD analysis. The radius of the circle represents the region of confidence (95%).

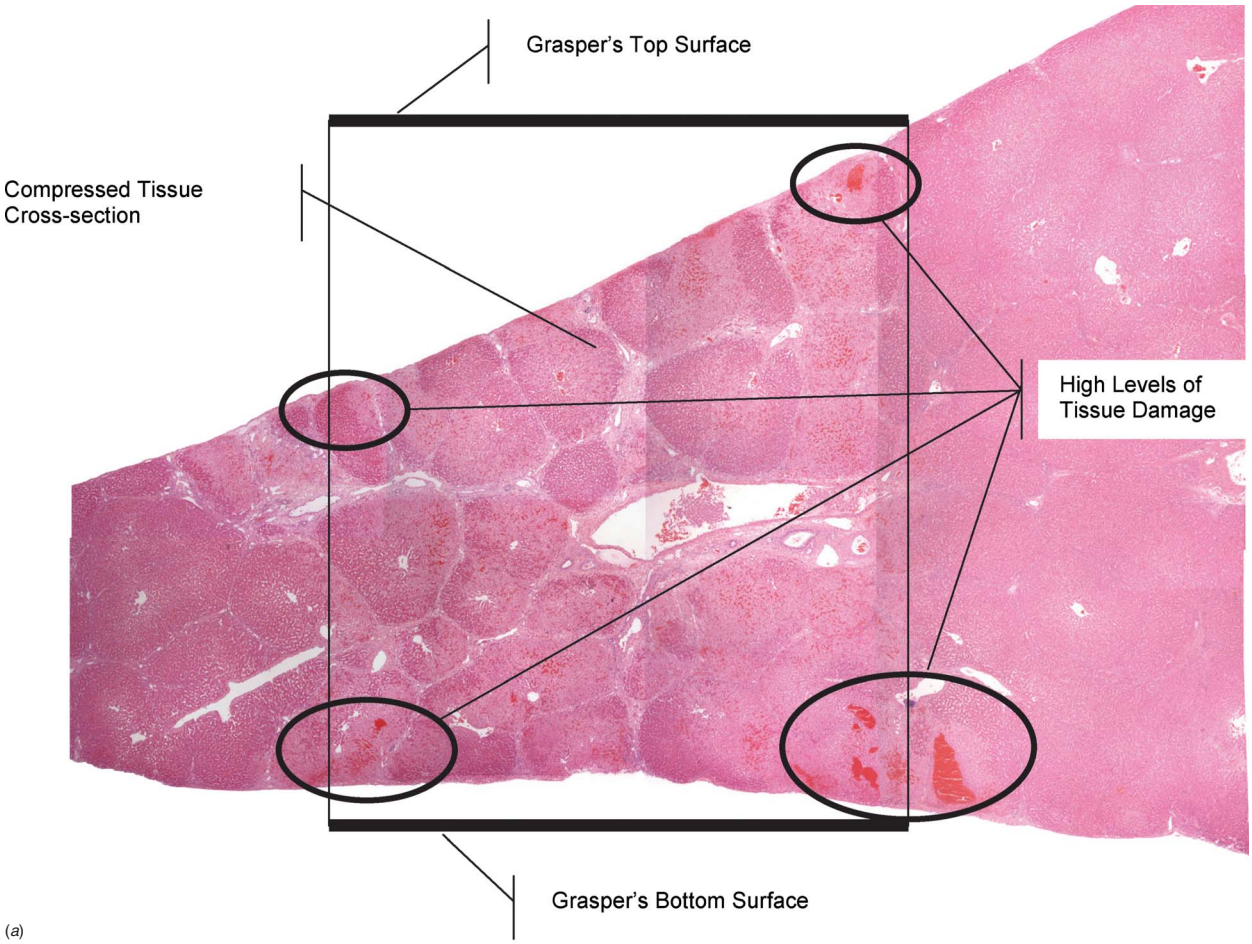

(*a*)

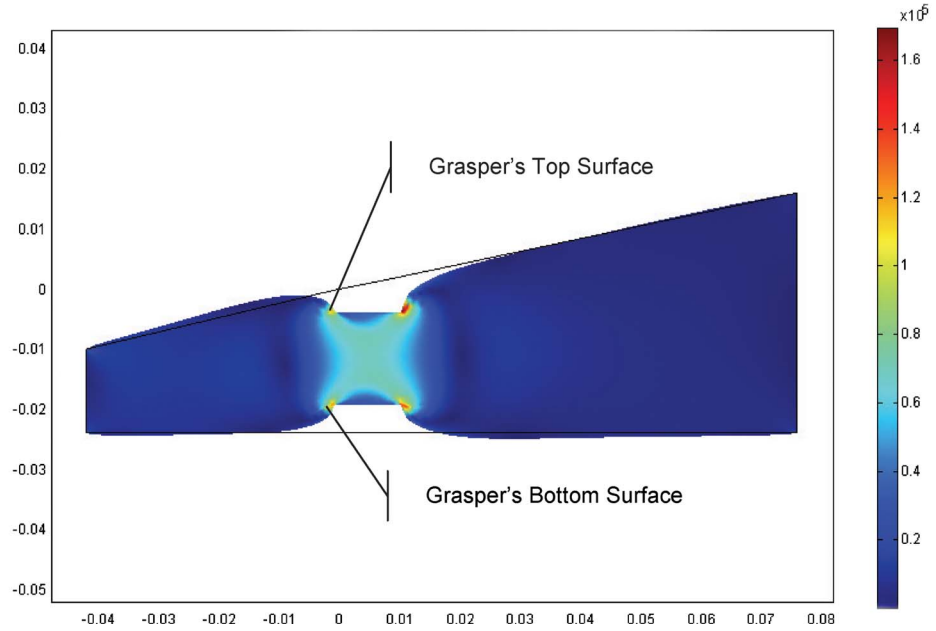

(*b*)

Fig. 11 The liver response to compression loads of 40% strain. (*a*) A cross section of a liver generated as an assembly of multiple tissue slices using standard pathological techniques following an application of compression strain by a Babcock grasper attached to the MEG. Vascular tissue damage is indicated by dark red areas across the tissue slices. The horizontal arrow indicates the approximate span of the grasper jaws. (*b*) Von Mises stress distribution and the displaced cross section of liver as predicted by a linear FEM. The geometrical dimensions are expressed in meters and stresses are expressed in Pascals.

the tissues' response to typical loading conditions in minimally invasive surgery. In that respect, the results reported in this study represent only one axis (dimension) of the tissue's triaxial response. However, it should be emphasized that given the inherent dependencies between the three dimensions, the two unloaded dimensions are reflected in the dimension under study here. In addition, the dimension under study is the very same dimension that the surgeon is exposed to as he or she palpates the tissue with standard surgical tools. Moreover, one may note that one underlying assumption of the elastic model was that the compression stresses are zero at zero strain. This initial condition limits the reported elastic model to incorporate the soft tissues' residual stresses due to hydration and natural internal boundary conditions, which in turn limits the model to accurately predict the tissues' stress response to small strains. This limitation is diminished for large strains, which are what surgeons typically apply during tissue manipulation.

Three major aspects of tissue's acute response to injury include cellular changes, inflammation, and the consequences of vascular damage. As part of a pilot study, the MEG was used to apply compressive loads to porcine liver tissue that was exposed to 30 s of compression load of an average nominal stress of 197 kPa, which corresponded to an overall strain of 40%. Figure 11(*a*) depicts a cross section of stressed liver generated as an assembly of multiple individual images from a tissue section produced by standard slicing and H&E staining techniques used in pathology. One may note substantial indications of tissue damage due to high stress concentrations at the edges of the grasper's tips. Figure 11(*b*) depicts the Von Mises stress distribution predicted by a linear finite element model (FEM FEMLAB) of the liver with plane strain assumptions. The model has the same geometrical dimensions as the liver specimen under study and was loaded with a compression strain of 40% with the following tissue properties: density $\rho=1.04$ kg/L, Young's modulus $E=150$ kPa, and Poisson's ratio $\gamma=0.45$. The boundary conditions along the outer edges of the liver FEM were fixed, and vertical displacements corresponding to 40% strain were applied to the nodes under the surfaces of the grasper. One may note that the tissue damage generated at the edge of the grasper due to high stress concentrations is predicted by the finite element model. Future studies will further study tissue damage mechanisms of internal organs as a result of loading regimes generated during minimally invasive surgery as well as nonlinear modeling of the corresponding organs. The database reported in this study will be useful to create accurate tissue models.

Acknowledgment

This research was funded by a major grant from U.S. Surgical (formerly a division of Tyco, Inc.) to the University of Washington Center for Videoendoscopic Surgery (CVES), a gift from Washington Research Foundation Capital, and a graduate fellowship provided by the Whitaker Foundation.

The authors wish to thank Dr. David Nuckley and Dr. Randy Ching of the University of Washington Applied Biomechanics Laboratory for their help in performing the tests of the postmortem tissues with the MTS machine, and to Catherine Westergaard of the CVES. We also thank UW surgical fellows Dr. Andy Isch and Dr. Todd Kellogg for their assistance with the in vivo experiments.

References

[1] Madhani, A. J., Niemeyer, G., and Salisbury, J. K., Jr., 1998, "The Black Falcon: A Teleoperated Surgical Instrument for Minimally Invasive Surgery," *IEEE/RSJ International Conference on Intelligent Robots and Systems*, New York, Vol. 2, pp. 936–944.

[2] Fung, Y. C., 1993, *Biomechanics: Mechanical Properties of Living Tissues*, 2nd ed., Springer, New York.

[3] Fung, Y. C., 1967, "Elasticity of Soft Tissues in Simple Elongation," Am. J. Physiol., **213**(6), pp. 1532–1544.

[4] Yamada, H., 1973, *Strength of Biological Materials*, Krieger, New York.

[5] Tay, B. K., Kim, J., and Srinivasan, M. A., 2006, "In Vivo Mechanical Behavior of Intra-Abdominal Organs," IEEE Trans. Biomed. Eng., **53**(11), pp. 2129–2138.

[6] Kerdok, A. E., Ottensmeyer, M. P., and Howe, R. D., 2006, "Effects of Perfusion on the Viscoelastic Characteristics of Liver," J. Biomech., **39**(12), pp. 2221–2231.

[7] Yoganandan, N., Pintar, F. A., and Maltese, M. R., 2001, "Biomechanics of Abdominal Injuries," Crit. Rev. Biomed. Eng., **29**(2), pp. 173–246.

[8] Rouhana, S. W., 1993, "Biomechanics of Abdominal Trauma," in *Accidental Injury: Biomechanics and Prevention*, A. M. Nahum and J. W. Melvin, eds., Springer-Verlag New York, pp. 391–428.

[9] Liu, Z., and Bilston, L., 2000, "On the Viscoelastic Character of Liver Tissue: Experiments and Modelling of the Linear Behaviour," Biorheology, **37**(3), pp. 191–201.

[10] Arbogast, K. B., Thibault, K. L., Pinheiro, B. S., Winey, K. I., and Margulies, S. S., 1997, "A High-Frequency Shear Device for Testing Soft Biological Tissues," J. Biomech., **30**(7), pp. 757–759.

[11] Dokos, S., LeGrice, I. J., Smaill, B. H., Kar, J., and Young, A. A., 2000, "A Triaxial-Measurement Shear-Test Device for Soft Biological Tissues," ASME J. Biomech. Eng., **122**(5), pp. 471–478.

[12] Gao, C. W., and Gregersen, H., 2000, "Biomechanical and Morphological Properties in Rat Large Intestine," J. Biomech., **33**(9), pp. 1089–1097.

[13] Gregersen, H., Emery, J. L., and McCulloch, A. D., 1998, "History-Dependent Mechanical Behavior of Guinea-Pig Small Intestine," Ann. Biomed. Eng., **26**(5), pp. 850–858.

[14] Carter, F. J., Frank, T. G., Davies, P. J., and Cuschieri, A., 2000, "Puncture Forces of Solid Organ Surfaces," Surg. Endosc, **14**(9), pp. 783–786.

[15] Carter, F. J., Frank, T. G., Davies, P. J., McLean, D., and Cuschieri, A., 2001, "Measurements and Modelling of the Compliance of Human and Porcine Organs," Med. Image Anal., **5**(4), pp. 231–236.

[16] Davies, P. J., Carter, F. J., and Cuschieri, A., 2002, "Mathematical Modelling for Keyhole Surgery Simulations: A Biomechanical Model for Spleen Tissue," IMA J. Appl. Math., **67**, pp. 41–67.

[17] Tamura, A., Omori, K., Miki, K., Lee, J. B., Yang, K. H., and King, A. I., 2002, "Mechanical Characterization of Porcine Abdominal Organs," *46th Stapp Car Crash Conference*, Vol. 46, pp. 55–69.

[18] Melvin, J. W., Stalnaker, R. L., Roberts, V. L., and Trollope, M. L., 1973, "Impact Injury Mechanisms in Abdominal Organs," *Proceedings of the 17th Stapp Car Crash Conference*, pp. 115–126.

[19] Zheng, Y. P., Mak, A. F. T., and Lue, B., 1999, "Objective Assessment of Limb Tissue Elasticity: Development of a Manual Indentation Procedure," J. Rehabil. Res. Dev., **36**(2), pp. 71–85.

[20] Zheng, Y. P., and Mak, A. F. T., 1999, "Extraction of Quasi-Linear Viscoelastic Parameters for Lower Limb Soft Tissues from Manual Indentation Experiment," ASME J. Biomech. Eng., **121**(3), pp. 330–339.

[21] Pathak, A. P., Silver, T. M. B., Thierfelder, C. A., and Prieto, T. E., 1998, "A Rate-Controlled Indentor for In Vivo Analysis of Residual Limb Tissues," IEEE Trans. Rehabil. Eng., **6**(1), pp. 12–20.

[22] Brouwer, I., Ustin, J., Bentley, L., Sherman, A., Dhruv, N., and Tendick, F., 2001, "Measuring In Vivo Animal Soft Tissue Properties for Haptic Modeling in Surgical Simulation," *Medicine Meets Virtual Reality, Newport Beach, CA, Jan. 24–27*, Stud. Health Technol. Inform., **81**, pp. 69–74.

[23] Ottensmeyer, M. P., and Salisbury, J., 2000, "In-Vivo Mechanical Tissue Property Measurement for Improved Simulations," Proc. SPIE, **4037**, pp. 286–293.

[24] Kalanovic, D., Ottensmeyer, M. P., Gross, J., Buess, G., and Dawson, S. L., 2003, "Independent Testing of Soft Tissue Viscoelasticity Using Indentation and Rotary Shear Deformations," *Medicine Meets Virtual Reality*, Newport Beach, CA, Jan. 22–25; Stud. Health Technol. Inform., **94**, pp. 137–143.

[25] Bicchi, A., Canepa, G., De, R. D., Iacconi, P., and Scillingo, E. P., 1996, "A Sensor-Based Minimally Invasive Surgery Tool for Detecting Tissue Elastic Properties," *Proceedings 1996 IEEE International Conference on Robotics and Automation*, New York, Vol. 1, pp. 884–888.

[26] Morimoto, A. K., Foral, R. D., Kuhlman, J. L., Zucker, K. A., Curet, M. J., Bocklage, T., MacFarlane, T. I., and Kory, L., 1997, "Force Sensor for Laparoscopic Babcock," *Medicine Meets Virtual Reality*, Stud. Health Technol. Inform., **39**, pp. 354–361.

[27] Greenish, S., Hayward, V., Chial, V., Okamura, A., and Steffen, T., 2002, "Measurement, Analysis, and Display of Haptic Signals During Surgical Cutting," Presence: Teleoperators and Virtual Environments, **11**(6), pp. 626–651.

[28] Brown, J. D., Rosen, J., Longnion, J., Sinanan, M., and Hannaford, B., 2001, "Design and Performance of a Surgical Tool Tracking System for Minimally Invasive Surgery," *ASME International Mechanical Engineering Congress and Exposition*, New York, Nov. 11–16; Adv. Bioeng., **51**, pp. 169–170.

[29] Rosen, J., Brown, J. D., Barreca, M., Chang, L., Hannaford, B., and Sinanan, M., 2002, "The Blue DRAGON—A System for Monitoring the Kinematics and the Dynamics of Endoscopic Tools in Minimally Invasive Surgery for Objective Laparoscopic Skill Assessment," *Medicine Meets Virtual Reality*, Newport Beach, CA, Jan. 23–26; Stud. Health Technol. Inform., **85**, pp. 412–418.

[30] Rosen, J., Brown, J. D., Barreca, M., Chang, L., Sinanan, M., and Hannaford, B., 2002, "The Blue DRAGON—A System for Measuring the Kinematics and the Dynamics of Minimally Invasive Surgical Instruments In-Vivo," *2002 IEEE International Conference on Robotics and Automation*, Washington, DC, Vol. 2, pp. 1876–1881.

[31] Rosen, J., Hannaford, B., MacFarlane, M. P., and Sinanan, M. N., 1999, "Force Controlled and Teleoperated Endoscopic Grasper for Minimally Invasive Surgery—Experimental Performance Evaluation," IEEE Trans. Biomed. Eng.,

46(10), pp. 1212–1221.
[32] Brown, J. D., Rosen, J., Moreyra, M., Sinanan, M., and Hannaford, B., 2002, "Computer-Controlled Motorized Endoscopic Grasper for In Vivo Measurement of Soft Tissue Biomechanical Characteristics," *Medicine Meets Virtual Reality*, Newport Beach, CA, Jan. 23–26; Stud. Health Technol. Inform., **85**, pp. 71–73.
[33] Brown, J. D., Rosen, J., Kim, Y. S., Chang, L., Sinanan, M. N., and Hannaford, B., 2003, "In-Vivo and In-Situ Compressive Properties of Porcine Abdominal Soft Tissues," *Medicine Meets Virtual Reality*, Newport Beach, CA, Jan. 22–25; Stud. Health Technol. Inform., **94**, pp. 26–32.
[34] Brown, J. D., Rosen, J., Sinanan, M. N., and Hannaford, B., 2003, "In-Vivo and Postmortem Compressive Properties of Porcine Abdominal Organs," *MICCAI 2003*, Montreal, Canada; Lect. Notes Comput. Sci., **2878**, pp. 238–245.
[35] Mkandawire, C., Ledoux, W., Sangeorzan, B., and Ching, R., 2001, "A Quasi-Linear Viscoelastic Model of Foot-Ankle Ligaments," *25th Annual Meeting of the American Society of Biomechanics*, University of California-San Diego, San Diego, CA, Aug. 8–11, 409–410.
[36] Woo, S. L., Simon, B. R., Kuei, S. C., and Akeson, W. H., 1980, "Quasi-Linear Viscoelastic Properties of Normal Articular Cartilage," ASME J. Biomech. Eng., **102**(2), pp. 85–90.
[37] Mow, V. C., Kuei, S. C., and Armstrong, C. G., 1980, "Biphasic Creep and Stress Relaxation of Articular Cartilage in Compression: Theory and Experiments," ASME J. Biomech. Eng., **102**(1), pp. 73–84.
[38] Ateshian, G. A., Warden, W. H., Kim, J. J., Grelsamer, R. P., and Mow, V. C., 1997, "Finite Deformation Biphasic Material Properties of Bovine Articular Cartilage from Confined Compression Experiments," J. Biomech., **30**(11/12), pp. 1157–1164.
[39] DiSilvestro, M. R., and Suh, J. K., 2001, "A Cross-Validation of the Biphasic Poroviscoelastic Model of Articular Cartilage in Unconfined Compression, Indentation, and Confined Compression," J. Biomech., **34**(4), pp. 519–525.
[40] DiSilvestro, M. R., Qiliang, Z., Marcy, W., Jurvelin, J. S., and Jun, K. F. S., 2001, "Biphasic Poroviscoelastic Simulation of the Unconfined Compression of Articular Cartilage: I-Simultaneous Prediction of Reaction Force and Lateral Displacement," ASME J. Biomech. Eng., **123**(2), pp. 191–197.
[41] DiSilvestro, M. R., Qiliang, Z., and Jun, K. F. S., 2001, "Biphasic Poroviscoelastic Simulation of the Unconfined Compression of Articular Cartilage: II-Effect of Variable Strain Rates," ASME J. Biomech. Eng., **123**(2), pp. 198–200.
[42] Fortin, M., Soulhat, J., Shirazi-Adl, A., Hunziker, E. B., and Buschmann, M. D., 2000, "Unconfined Compression of Articular Cartilage: Nonlinear Behavior and Comparison with a Fibril-Reinforced Biphasic Model," ASME J. Biomech. Eng., **122**(2), pp. 189–195.
[43] Suh, J. K., and Spilker, R. L., 1994, "Indentation Analysis of Biphasic Articular Cartilage: Nonlinear Phenomena Under Finite Deformation," ASME J. Biomech. Eng., **116**(1), pp. 1–9.
[44] Lai, W. M., Hou, J. S., and Mow, V. C., 1991, "A Triphasic Theory for the Swelling and Deformation Behaviors Behaviors of Articular Cartilage," ASME J. Biomech. Eng., **113**(3), pp. 245–258.
[45] Brown, J. D., Rosen, J., Chang, L., Sinanan, M. N., and Hannaford, B., 2004, "Quantifying Surgeon Grasping Mechanics in Laparoscopy Using the Blue DRAGON System," *Medicine Meets Virtual Reality*; Stud. Health Technol. Inform., **98**, pp. 34–36.
[46] Farshad, M., Barbezat, M., Flueler, P., Schmidlin, F., Graber, P., and Niederer, P., 1999, "Material Characterization of the Pig Kidney in Relation With the Biomechanical Analysis of Renal Trauma," J. Biomech., **32**(4), pp. 417–425.
[47] Wang, J., Brienza, D. M., Bertocci, G., and Karg, P., 2001, "Stress Relaxation Properties of Buttock Soft Tissues: In Vivo Indentation Test," *Proceedings of the RESNA 2001 Annual Conference*, NV, Reno, Jun. 22–26, pp. 391–393.
[48] Simon, B. R., Coats, R. S., and Woo, S. L., 1984, "Relaxation and Creep Quasilinear Viscoelastic Models for Normal Articular Cartilage," ASME J. Biomech. Eng., **106**(2), pp. 159–164.